# A Powered Finger–Thumb Wearable Hand Exoskeleton With Self-Aligning Joint Axes

Marco Cempini, *Student Member, IEEE*, Mario Cortese, and Nicola Vitiello, *Member, IEEE*

***Abstract*—In recent years, the robotic research area has become extremely prolific in terms of wearable active exoskeletons for human body motion assistance, with the presentation of many novel devices, for upper limbs, lower limbs, and the hand. The hand shows a complex morphology, a high intersubject variability, and offers limited space for physical interaction with a robot: as a result, hand exoskeletons usually are heavy, cumbersome, and poorly usable. This paper introduces a novel device designed on the basis of human kinematic compatibility, wearability, and portability criteria. This hand exoskeleton, briefly HX, embeds several features as underactuated joints, passive degrees of freedom ensuring adaptability and compliance toward the hand anthropometric variability, and an *ad hoc* design of self-alignment mechanisms to absorb human/robot joint axes misplacement, and proposes a novel mechanism for the thumb opposition. The HX kinematic design and actuation are discussed together with theoretical and experimental data validating its adaptability performances. Results suggest that HX matches the self-alignment design goal and is then suited for close human–robot interaction.**

***Index Terms*—Design, exoskeleton, finger, hand, mechanic, self-alignment, thumb, wearability.**

## I. Introduction

EXOSKELETONS are wearable robotic machines originally studied for human body powered assistance in heavy-duty and/or repetitive tasks. Assistive technologies gained relevance in industrial and military application, leading to a number of prototypes, patents, and commercial products [1]– [2]. The possibility of a close-coupled human–robot system also led to an evolution in the biomedical field, with the use in research and clinical environments of many robots for the rehabilitation of impaired people [3]–[5].

From a general point of view, the integration of a wearable robot with a human user may follow the *hybridization design principle* [6]. In healthy condition, the human sensory motor apparatus provides a high sensitiveness, fast reactions to sudden environmental variations, and the natural trend to implement joints motion synergies toward an efficient and reliable execution of task (e.g., reach-to-grasp or walking gait); all these features are hard to model and implement in the robotic counterpart. Conversely, the exoskeleton is demanded to provide additional power and to follow the intended human movement while sustaining an additional payload.

Similarly, rehabilitation robots should aid the patient in restoring a lost mobility. End-point external machines [7] cannot discriminate whether the subject is regaining motion skill at the impaired joint, or is using other muscles and body parts [8]. Exoskeletons instead provide the therapist with specific data for each anatomical joint, which are also important in assessing the recovery of functional motion synergies [9].

The complementary features of the human and the robot systems are not sufficient for their efficient integration, it is also necessary to foster the *compatibility* of the two: this raises several issues in the physical human–robot interaction (pHRI). The need to match the complexity and the intersubject variability of human skeletal kinematics [10]–[13], the requirements of a low-encumbrance and lightweight device, and the minimal possible hindering effects on the user limbs, like compression forces along the bones or high pressure on the skin [5], are the most challenging features asked to an exoskeletal system. Moreover, for a good compatibility it is desirable that the user had an high level of "confidence" in the worn device. Hence, crucial aspects are also the *dependability* (how much the platform can be relied on [14]) and the *usability* (the level of easiness, comfort, and satisfaction with which the user–robot interaction takes place [5]).

In the exoskeleton, state-of-the-art devices for hand rehabilitation or assistance[1] are among the most addressed [15]. Due to the relevance of hand motor functions in activities of daily living, and the strong connection with the nervous system [16], the pHRI needs to be finely tuned, especially for what concerns the compatibility. Two are the main exoskeleton design approaches: fixed-frame platforms or portable devices. Devices based on the former [17], [18] are precise, robust, and can provide the high forces required in many rehabilitation practices, but are extremely heavy and cumbersome. A reduction in size and complexity may be obtained through kinematic simplification, replicating only basic motions—such as power grasp [19]. In all these cases, however, the forearm and wrist are constrained on a rigid frame, and orientation of the hand is not allowed, thus functional tasks (pick-and-lift, or reach-and-grasp) cannot be properly addressed. Hence, it is not correct to speak about human–robot integration: in fact they are mostly used in master–slave rehabilitative treatments with a passive user.

Manuscript received November 6, 2013; revised March 26, 2014; accepted March 31, 2014. Date of publication April 29, 2014; date of current version October 24, 2014. Recommended by Technical Editor W. J. Zhang. This work was supported in part by the EU within the WAY Project ("Wearable interfaces for hand function recoverY," FP7-ICT-Ch5 G.A. 288551) and in part by the Italian Ministry of Economic Development within the AMULOS Project (ADVANCED MULOS, Contract MI01_00319), and in part by the Regione Toscana under the Health Regional Research Program 2009 within the project EARLYREHAB.

The authors are with the BioRobotics Institute, Scuola Superiore di Studi Universitari e di Perfezionamento Sant'Anna, 56025 Pontedera, Italy (e-mail: m.cempini@sssup.it; m.cortese@sssup.it; n.vitiello@sssup.it).

Color versions of one or more of the figures in this paper are available online at http://ieeexplore.ieee.org.

Digital Object Identifier 10.1109/TMECH.2014.2315528

[1] A different field deals with the teleoperation/haptic, where the hand/fingers motions are detected and, consequently, a feedback is sent to the user. The devices are mostly passive and carry feedback element, typically on the fingertip.

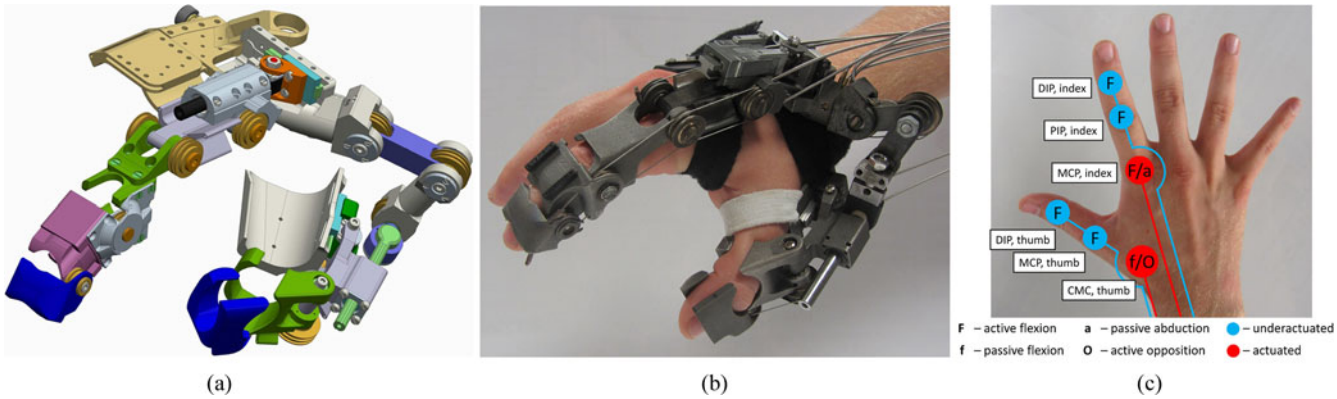


Fig. 1. HX system: (a) CAD of the device. (b) System worn on the hand. (c) Anatomical joints and motions addressed by the device.

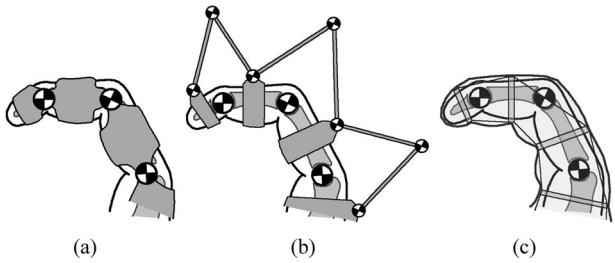


Fig. 2. Different solutions for finger exoskeletons. (a) Replica of the finger structure with an external series of shell linkages (see [21]). (b) Additional passive DoFs, the most recurrent solution [31], [35], [36]. (c) "Soft" solution with structure-less frame actuated by tendons or pneumatic tubes [28].

Wearable devices are more challenging. Their architecture can be classified according to Fig. 2 [15]. The simpler choice is to replicate each of the addressed joint with an external homologous structure, Fig. 2(a) [20], [21]. The main limitation of this design is the possibility of a misalignment between the human and robot rotation axes: this issue is prevented by using nonanthropomorphic structures with redundant degrees of freedom (DoFs) [22]. The multijoint design [see Fig. 2(b)] is the most employed [23]–[26], but the high number of DoFs leads to augmented inertia of the aiding device. Moreover, when a broad range of movement (RoM) is requested, the robotic chain results into a someway "huge" mechanical structure. Solutions like [27] use an exoskeleton external to the finger, but with center of motion matching the user phalangeal joints, thus are conceptually analogous to the case of Fig. 2(a). It is worth noting that in portable exoskeletons, the thumb opposition has never been directly addressed, despite its relevance in grasping and handling. Another option is that of *soft-exoskeleton* [see Fig. 2(c)] where the robot structure is highly deformable and only transmits the actuation motions to the overall human hand via flexible elements [28]– [29]. These devices show very high wearability and adaptability. Conversely, the main limitation is in the admissible range of applied forces: without a support structure, compression loads arise along the user bones, thus exerted forces cannot be as high as desired.

As previously explained, a well-known issue is that of *alignment* between the robotic and human joints: this problem has been repeatedly stressed in the literature, as it causes strong discomfort in the user and mines the safety and efficiency of the device [10], [22], [30]. It is possible to distinguish two kinds of misalignment countermeasures. The first is the *compensation* kind [8]: other DoFs or lability *external* to the basic architecture are recruited to recover the aligned state. This is the case of Fig. 2(a) and (c), where if some misalignment occurs, deformation of the finger tissue or of the exoskeleton soft structure will compensate. On the scale size of human hand, it is hard to manage such contributes, since adjustments should be provided without adding backlash or worsening the device efficiency [24], [27]. The second is the *self-alignment* approach [13]: inside the basic exoskeleton architecture there are elements (active or passive) properly designed to address the misalignments. This is the case of Fig. 2(b), with the use of redundant DoFs [31], and is the same approach adopted in this paper. The self-alignment property [13] can be addressed as a particular case of the self-recovery one, further generalized into the resilient system concept [32]. By resilient, it is meant that the system can recover to a balanced state: in the case of physical interaction between a human user and a wearable robot, the balanced state corresponds to the alignment between the actuated robotic joint and the anatomical one.

This paper presents the design and development of a novel wearable hand exoskeleton, briefly HX [33], [34] facing all the aforementioned issues: HX is a thumb–finger hand exoskeleton (see Fig. 1), exploiting proper mechanisms to guarantee human/robot self-alignment while providing force/motions to the carpal, metacarpal, and phalangeal joints. An early work related to HX was presented in [34]: here a more exhaustive description of the index–finger module is given along with a detailed experimental validation of the design assumptions; the 3-D motion of the thumb is here presented for the first time.

This paper is organized as follows. Section II presents the framework underlying the design of HX. Section III explains actuation means. Section IV reports an experimental validation of the pHRI performances. Discussion, conclusive remarks, and future perspectives are given in Section V.

## II. Rationale of Kinematic Design for HX

A complete review of state-of-the-art hand exoskeletons is given in [15]: despite the many implemented designs, the

literature lacks an homogeneous treatment for the design of exoskeleton mechanics. An emerging field of the machine design exposes the concept of resilience [32], defined as the inherent ability of a system to go back to a functional state after a failure. The functional state of a wearable robot can be identified as the alignment between the exoskeleton and the human joint axes, since in this condition the robot actuation is correctly transferred to the correspondent body segment. In order to be resilient, the exoskeleton must react to the misaligned state (due to the not modeled anatomical joint morphology, slipping of the exoskeleton garments, or the mobilization of other joint than the ones of interest): introduction of passive DoFs in the exoskeleton architecture is a widely accepted way to comply for such effect [23]–[26], [31], [35], [36].

The self-alignment methodology exposed in [13] first provided a quantitative way[2] to analyze simultaneously and conjugate the exoskeleton effectiveness (i.e., the torque effectively delivered to the human joints) with the human compatibility (i.e., the compatibility toward a misaligned state). The advantage of such methodology is that it returns the definition of the actuation torques, stressing which joints are active and which are passive into the exoskeleton. In a true hybridization context [6], active DoFs allow the actuation and transmission of robot power toward the human limb, while passive DoFs allow the human system to decide where the joints axes are located. Proposed methodology is hereafter recapped.

### A. Framework for Self-Alignment of Human and Robotic Chains

Basically, the human joint is modeled as a "main" DoF $\tilde{\boldsymbol{q}}$, separating two body segments, the "proximal" and the "distal" links; the exoskeleton is meant to connect such links and provides *actions* (torque or motion). If the positions of the $\tilde{\boldsymbol{q}}$ axes are exactly known, then the system is always in a perfectly aligned state, Fig. 2(a). This is not a realistic case: misalignment is represented by a set of additional DoFs into the human chain $\boldsymbol{\delta}$ which makes the $\tilde{\boldsymbol{q}}$ axes deviate from the main model. The $\boldsymbol{\delta}$ are then called "misaligning" human DoFs, or "deviations," and represent the major uncertainties relative to the particular case under study (e.g., slippery of the exoskeleton garments, tilting of the skeletal joint, generic misalignment). In order to recover the aligned state, the exoskeleton uses a multitude of joints $\boldsymbol{q}$. Under proper assumptions[2] it is possible to split $\boldsymbol{q}$ between "controlling" and "adaptive" robotic joints,

$$\boldsymbol{q} = \begin{bmatrix} \boldsymbol{q}_c \\ \boldsymbol{q}_a \end{bmatrix}, \dim(\boldsymbol{q}) = n = \dim(\tilde{\boldsymbol{q}}) + \dim(\boldsymbol{\delta}) \Rightarrow$$
$$(\boldsymbol{\delta}, \tilde{\boldsymbol{q}}) = f(\boldsymbol{q}) \Leftrightarrow \begin{cases} \tilde{\boldsymbol{q}} = g(\boldsymbol{q}_c) \\ \boldsymbol{\delta} = h(\boldsymbol{q}_c, \boldsymbol{q}_a) \end{cases} \quad (1)$$

in a way such that the human main joint posture is purely controlled by $\boldsymbol{q}_c$, whichever the values of $\boldsymbol{q}_a$ absorbing the contingent deviations. From the kinematic laws (1), the existence of a dual relation involving the applied forces/torques (kineto-static duality [13]) can be shown, which for the present case becomes[2]

$$\begin{cases} \dot{\tilde{\boldsymbol{q}}} = G(\boldsymbol{q})\dot{\boldsymbol{q}}_c \\ \dot{\boldsymbol{\delta}} = H_1(\boldsymbol{q})\dot{\boldsymbol{q}}_a + H_2(\boldsymbol{q})\dot{\boldsymbol{q}}_c \end{cases}, \quad \begin{cases} \boldsymbol{\tau}_c = G^{\mathsf{T}}(\boldsymbol{q})\tilde{\boldsymbol{\tau}} + H_2^{\mathsf{T}}(\boldsymbol{q})\boldsymbol{\tau}_\delta \\ \boldsymbol{\tau}_a = H_1^{\mathsf{T}}(\boldsymbol{q})\boldsymbol{\tau}_\delta \end{cases} \quad (2)$$

where $\boldsymbol{\tau}_c$, $\boldsymbol{\tau}_a$, $\boldsymbol{\tau}_\delta$, and $\tilde{\boldsymbol{\tau}}$ are the torques applied, respectively, to the $\boldsymbol{q}_c$, $\boldsymbol{q}_a$, $\boldsymbol{\delta}$, and $\tilde{\boldsymbol{q}}$ joints. The functions $g$, $h$ represent the human–robot kinematic coupling, and the matrices $G$, $H_1$, and $H_2$ are their derivatives with respect to the robotic joints $\boldsymbol{q}_c$ and $\boldsymbol{q}_a$ postures, namely Jacobian matrices. It is possible to define proper conditions[2] for which the exoskeleton can nullify the "deviations" torques, $\boldsymbol{\tau}_\delta = \boldsymbol{0}$ and simultaneously control the joint torques $\tilde{\boldsymbol{\tau}}$, thus effectively managing the power delivered to the human joint without undesired reactions.

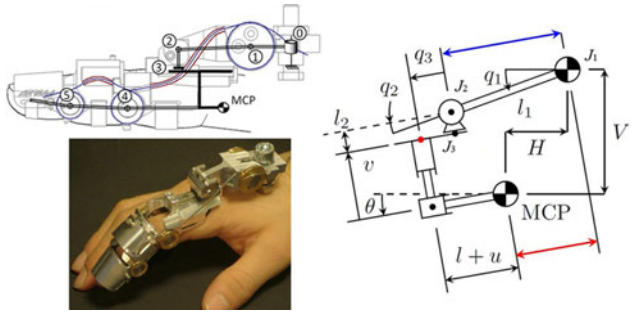


Fig. 3. Multijoint kinematic solutions from [31]. MCP chain is composed by joints 1-2-3. The MCP joint f/e angle is indicated by $\theta$. Two additional joints stand between the exoskeleton end-effector (red dot) and the MCP joint, $u$ aligned with the phalanx, and $v$ normal to it.

### B. Finger Kinematic Design

The design of a finger exoskeleton[3] has been object of several works. Finger anatomy is here described [37]:

1) the index has a planar structure developed on the flexion–extension (f/e) plane, which divides it symmetrically;
2) joints are of revolute kind, with axes normal to the f/e plane, and are indicated by the MCP, PIP, and DIP acronyms [respectively MetaCarpo-Phalangeal, Phalangeal-InterPhalangeal, and Distal-InterPhalangeal, Fig. 2(a)];
3) MCP joint allows also for the *abduction-adduction* (a/a) movement, a rotation around an axis normal to the f/e one and to the hand dorsi-palmar plane.

As a matter of fact, (2) can be applied for any exoskeletal chain with redundant DoFs. The usefulness of the methodology in [13] depends on how the deviations $\boldsymbol{\delta}$ are modeled. Before explaining our strategy, we will present meaningful examples from the state of the art.

HANDEXOS [31] is a finger exoskeleton with redundant DoFs for the MCP. Chain kinematics is a serial $\underline{R}RP$, laying on the f/e plane, with the last prismatic joint almost parallel to the first phalanx bone, Fig. 3. Motivation of this choice is mainly that the resultant force at the end-effector (see red dot in Fig. 3) may have only a normal force component, eliciting

[2]Details on the mathematical background can be found in [13].

[3]The targeted finger is often the index, as the more relevant and dexterous among the hand long fingers, but nomenclature is valid for all of them.

the MCP rotation without burdening the articulation. In order to analyze such requirement, two linear DoFs can be added: $u$, concerning the distance between the exoskeleton links and the MCP along the phalanx (thus taking into consideration the force along such direction, which the exoskeleton aims at nullify), and its orthogonal counterpart $v$. By doing so, the following kinematic relation holds (symbolism as in Fig. 3):

$$\begin{cases} \theta = q_1 + q_2 \\ v = l_1 \sin q_2 - H \sin(q_1+q_2) + V \cos(q_1+q_2) - l_2 \\ u = l_1 \cos q_2 - H \cos(q_1+q_2) - V \sin(q_1+q_2) + q_3 - l. \end{cases} \tag{3}$$

Since the MCP angle $\theta$ and the finger normal compression $v$ depend only on $q_1$ and $q_2$, we can split the human DoFs in $\tilde{\boldsymbol{q}} = [\theta, v]^\mathsf{T}$ and $\boldsymbol{\delta} = [u]$, achieving formulation (1) with $\boldsymbol{q}_c = [q_1, q_2]^\mathsf{T}$ and $\boldsymbol{q}_a = [q_3]$. Matrices $G$, $H_1$, and $H_2$ of (2) can be derived from (3)[4],

$$G = \frac{\partial \tilde{\boldsymbol{q}}}{\partial \boldsymbol{q}_c} = \begin{bmatrix} 1 & 1 \\ -Hc_{12} - Vs_{12} & l_1 c_2 - Hc_{12} - Vs_{12} \end{bmatrix}$$

$$H_1 = \frac{\partial \boldsymbol{\delta}}{\partial \boldsymbol{q}_a} = \left[\frac{\partial u}{\partial q_3}\right] = [1]$$

$$H_2 = \frac{\partial \boldsymbol{\delta}}{\partial \boldsymbol{q}_c} = \left[\frac{\partial u}{\partial q_1}, \frac{\partial u}{\partial q_2}\right] = [Hs_{12} - Vc_{12}, Hs_{12} - l_1 s_2 - Vc_{12}].$$

Being $H_1$ a constant square matrix, condition $\boldsymbol{\tau}_\delta = [F_u] = \mathbf{0}$ is satisfied by $\boldsymbol{\tau}_a = [\tau_3] = \mathbf{0}$, i.e., the prismatic guide must be passive, as in the HANDEXOS design. The actuation of joints 1 and 2 determines the wrench on the human joints,

$$\begin{bmatrix} T_1 \\ T_2 \end{bmatrix} = \boldsymbol{\tau}_c = G^\mathsf{T} \tilde{\boldsymbol{\tau}} + H_2^\mathsf{T} \boldsymbol{\tau}_\delta = \begin{bmatrix} 1 & -Hc_{12} - Vs_{12} \\ 1 & l_1 c_2 - Hc_{12} - Vs_{12} \end{bmatrix} \begin{bmatrix} T_\theta \\ F_v \end{bmatrix}.$$

HANDEXOS has only the first joint actuated ($T_2 = 0$), thus providing a net MCP joint torque

$$T_\theta = \left(1 - \frac{Hc_{12} + Vs_{12}}{l_1 c_2}\right) T_1 \Rightarrow \frac{T_\theta}{T_1} = 1 - \frac{Hc_\theta + Vs_\theta}{l_1 c_2}. \tag{4}$$

Formulation (4) is valid as long as $\det(G) = l_1 c_2 \neq 0$, which is guaranteed into the reasonable RoM $|q_2| > \frac{\pi}{2}$. Transmission is affected by a geometric factor, corresponding to the ratio between the red and blue lengths in Fig. 3: as $\theta$ increases, this ratio approaches the unity, thus lowering the efficiency.

Another example is the four-bar mechanism [24], [35], [36], used in exoskeleton with the human distal link as driven member, and by assuming as rigid frame the line connecting the human joint and the first exoskeleton joint, along the human proximal link. With reference to Fig. 4, exoskeleton joints $J_{2,3}$ are passive, and are used to match different wearer's size (one of the many possible source of misalignment). To analyze the

[4]In the following, we will adopt the common notation $s_i = \sin q_i$, $c_i = \cos q_i$. Multiple subscripts indicate summations of argument angles.

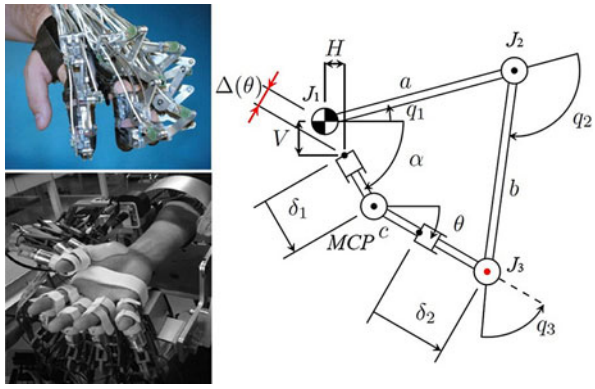


Fig. 4. Four-bar kinematic exoskeletons [24], [36], composed by three revolute joints (1, 2, 3) and two links ($a$, $b$). Remaining elements are human-related: since these are not controllable, their uncertainties and variations are represented by two additional prismatic DoFs. $H$, $V$, $\alpha$, and $c$ are constant.

coupled human–robot system, a two-element deviation $\boldsymbol{\delta}$ is introduced, representing the variations of the human-related linkages lengths. Kinematic coupling is expressed by (5), which show that the human joint $\tilde{\boldsymbol{q}} = [\theta]$ is linearly dependent on all three revolute joints angles $q_{1,2,3}$

$$\begin{cases} \theta = -(q_1 + q_2 + q_3) \\ \delta_1 \sin(\alpha - \theta) = a \sin(q_2 + q_3) + b \sin q_3 - \Delta(\theta) \\ (c + \delta_2) \sin(\alpha - \theta) = a \sin(q_1 + \alpha) + b \sin(q_1 + \alpha + q_2). \end{cases} \tag{5}$$

Since all the exoskeleton joints contribute to $\theta$, all of them should be accounted in the controlling set, $\boldsymbol{q}_c = [q_1, q_2, q_3]^\mathsf{T}$, $\boldsymbol{q}_a = \emptyset$. By direct calculations, matrices $G$ and $H_2$ and the torque relation are obtained

$$G = \frac{\partial \tilde{\boldsymbol{q}}}{\partial \boldsymbol{q}_c} = [1 \quad 1 \quad 1], \; H_2 = \frac{\partial \boldsymbol{\delta}}{\partial \boldsymbol{q}_c} = \begin{bmatrix} \frac{c_{\alpha-\theta}(as_{23} + bs_3)}{-s^2_{\alpha-\theta}} & \frac{as_{1\alpha} - bs_3 c_{\alpha-\theta}}{s^2_{\alpha-\theta}} & \frac{as_{1\alpha} + bs_{1\alpha 2}}{s^2_{\alpha-\theta}} \\ \frac{as_{23} + bs_3}{s^2_{\alpha-\theta}} & \frac{bs_3 - as_{1\alpha} c_{\alpha-\theta}}{s^2_{\alpha-\theta}} & \frac{c_{\alpha-\theta}(as_{1\alpha} + bs_{1\alpha 2})}{-s^2_{\alpha-\theta}} \end{bmatrix}$$

$$\begin{bmatrix} T_1 \\ T_2 \\ T_3 \end{bmatrix} = \boldsymbol{\tau}_c = G^\mathsf{T} \tilde{\boldsymbol{\tau}} + H_2^\mathsf{T} \boldsymbol{\tau}_\delta = \left[G^\mathsf{T}, H_2^\mathsf{T}\right] \begin{bmatrix} T_\theta \\ F_{\delta_1} \\ F_{\delta_2} \end{bmatrix}. \tag{6}$$

$H_2$ depends only on the angles between each of the four bars: $q_1 + \alpha$, $q_2$, $q_3$ and $\alpha - \theta$. If only the exoskeleton joint $J_1$ is actuated ($T_2 = T_3 = 0$) as in [24], (6) gives

$$T_\theta = T_1 \frac{a \sin(q_1 + \alpha) + b \sin(q_1 + \alpha + q_2)}{a \sin q_2 \sin(\alpha - \theta)} \sin q_3. \tag{7}$$

Equation (7) states that in order to control the torque $T_\theta$, all the angles must be accounted for; moreover, it becomes singular for $\theta = \alpha$. Instead, if all the $\boldsymbol{q}_c$ joints are actuated, it is possible to match the compatibility requirement $F_{\delta_{1,2}} = 0$

$$F_{\delta_1} = F_{\delta_2} = 0 \Rightarrow \boldsymbol{\tau}_c = G^\mathsf{T} \tilde{\boldsymbol{\tau}} \Rightarrow T_1 = T_2 = T_3 = T_\theta. \tag{8}$$

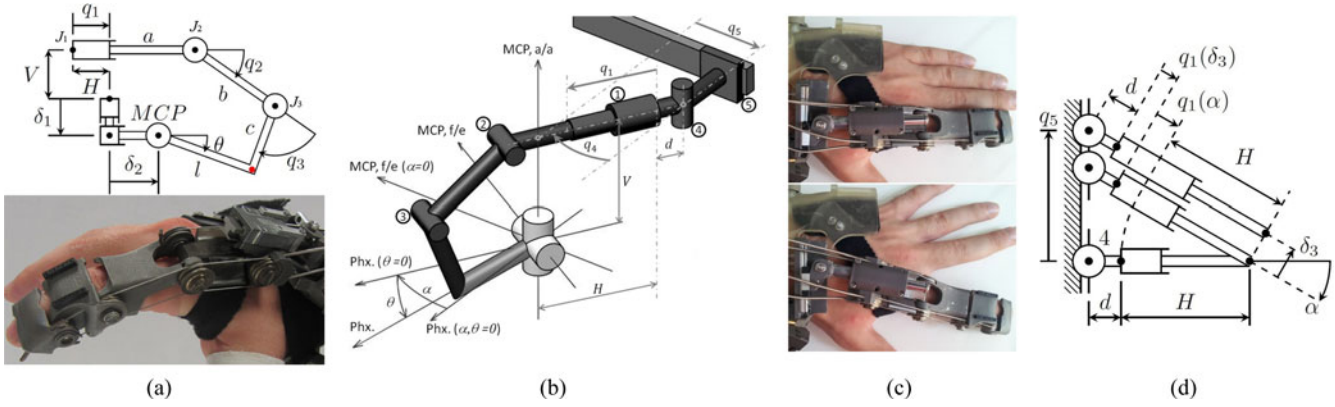


Fig. 5. HX exoskeleton, finger architecture [34]. (a) Self-alignment chain: the MCP joint center is subjected to varying displacements $\delta_{1,2}$. The kinematic is the same used in devices as [23], [25], however the way it is actuated makes a difference. (b) Isometric view of the full self-alignment chain: the MCP f/e, a/a axes, and the first phalanx direction are reported. $\theta$ and $\alpha$ are respectively the f/e and a/a angles. (c) Comparison between abducted/adducted finger. (d) Drawing showing the DoFs involved in the a/a motion (top view): this joints also absorb MCP displacement $\delta_3$, normal to the f/e plane. As a result, two additive terms $q_1(\alpha)$ and $q_1(\delta_3)$ arises in the passive joint 1.

Result (8) is much cleaner and simpler than (7): it implies that the four-bar mechanism should be used as a pure-torque transmission system, by actuating all its three revolute joints synchronously. The same conclusion was reached in [10], for an elbow exoskeleton, where a design employing three cable-driven pulleys actuated simultaneously embodied the aforementioned strategy.

Fig. 5 shows the HX finger module, early presented in [34]. HX uses a compound solution for the index finger joints, the kinematic chain being $P\underline{RR}\,\underline{RR}$. The latter $\underline{RR}$ joints address PIP and DIP, with a direct matching of the robotic joint on the human ones [see Fig. 2(a)]: identification of the anatomical axes is eased thanks to the full access to the finger sides, thus a compensation approach is sufficient to absorb misalignment. A soft Neoprene foam layer covering the inner side of the phalangeal links was added for this purpose. A self-alignment $P\underline{RR}$ chain is instead used for the MCP, since this joint axis is hardly recognizable due to the bones and articular capsule morphology [38]. With reference to Fig. 5, misalignment of the MCP instantaneous center are modeled by two linear joints $\delta_{1,2}$. Kinematic relations are

$$\begin{cases} \theta = q_2 + q_3 - \frac{\pi}{2} \\ \delta_1 = b\,s_2 + c\,s_{23} + l\,c_{23} - V \\ \delta_2 = q_1 - H + a + b\,c_2 + c\,c_{23} - l\,s_{23}. \end{cases} \tag{9}$$

Both robotic revolute joints $J_{2,3}$ concur to the MCP flexion angle $\tilde{\boldsymbol{q}} = [\theta]$, hence, $[q_2, q_3]^{\mathsf{T}} = \boldsymbol{q}_c$

$$G = \frac{\partial \tilde{\boldsymbol{q}}}{\partial \boldsymbol{q}_c} = [1 \quad 1], H_1 = \frac{\partial \boldsymbol{\delta}}{\partial \boldsymbol{q}_a} = \begin{bmatrix} 0 \\ 1 \end{bmatrix}$$

$$H_2 = \frac{\partial \boldsymbol{\delta}}{\partial \boldsymbol{q}_c} = \begin{bmatrix} b\,c_2 + c\,c_{23} - l\,s_{23} & c\,c_{23} - l\,s_{23} \\ -b\,s_2 - c\,s_{23} - l\,c_{23} & -c\,s_{23} - l\,c_{23} \end{bmatrix}. \tag{10}$$

A detailed solution for the case in which $G$ and $H_1$ are not square matrices, as in (10), can be found in [13]; the result is $\begin{bmatrix} \boldsymbol{\tau}_c \\ \boldsymbol{\tau}_a \end{bmatrix} = \begin{bmatrix} G^{\mathsf{T}} & H_2^{\mathsf{T}} \\ \mathbf{0} & H_1^{\mathsf{T}} \end{bmatrix} \begin{bmatrix} \tilde{\boldsymbol{\tau}} \\ \boldsymbol{\tau}_\delta \end{bmatrix} \Rightarrow \begin{bmatrix} T_2 \\ T_3 \\ F_1 \end{bmatrix} = \begin{bmatrix} 1 & b\,c_2 + c\,c_{23} - l\,s_{23} & -b\,s_2 - c\,s_{23} - l\,c_{23} \\ 1 & c\,c_{23} - l\,s_{23} & -c\,s_{23} - l\,c_{23} \\ 0 & 0 & 1 \end{bmatrix} \begin{bmatrix} T_\theta \\ F_{\delta_1} \\ F_{\delta_2} \end{bmatrix}$ and it shows that reactions $F_{\delta_{1,2}} = 0$ (i.e., freedom of movement of the MCP center position) can be achieved through

$$F_{\delta_1} = F_{\delta_2} = 0 \Rightarrow F_1 = 0, \quad T_2 = T_3 = T_\theta. \tag{11}$$

Result (11) is similar to (8). Indeed, in HX the two revolute joints $J_{2,3}$ are actuated simultaneously, in order to deliver a pure torque to the MCP joint (see Section III-A).

This is not the only novelty of HX: the axis of the passive prismatic guide $J_1$ is orthogonal to both the MCP f/e and a/a axes. Thus, its self-alignment function becomes twofold: it allows the joints $J_{2,3}$ to follow the human MCP center deviations, and allows the whole f/e structure to follow the a/a motion. For this latter purpose the $J_1$ base is supported with two additional DoFs, $J_4$ (revolute, parallel to the MCP a/a axis) and $J_5$ (prismatic, parallel to the radial-ulnar direction, Fig. 5). In addition this kinematic arrangement is also compatible toward deviations of the MCP center away from the exoskeleton f/e plane, $\delta_3$ in Fig. 5(d). In the end, HX will comply with any misplacement of the MCP joint axis.

Basing on Fig. 5(d), (9) is still valid if $q_1$ is replaced by $q_1 - q_1(\delta_3) - q_1(\alpha)$: complete kinematics becomes

$$\begin{cases} q_1(\alpha) = (d+H)\dfrac{1-\cos\alpha}{\cos\alpha} \; q_1(\delta_3) = \delta_3 \tan\alpha \\ q_4 = \alpha \; q_5 = \dfrac{\delta_3}{\cos\alpha} + (d+H)\tan\alpha \end{cases} \Rightarrow$$

$$\begin{cases} \theta = q_2 + q_3 + \frac{\pi}{2} \\ \alpha = q_4 \\ \delta_1 = b\,s_2 + c\,s_{23} + l\,c_{23} - V \\ \delta_2 = b\,c_2 + c\,c_{23} - l\,s_{23} - (d+H)c_4 - q_5 s_4 + q_1 + a + d \\ \delta_3 = q_5 c_4 - (d+H)s_4. \end{cases} \tag{12}$$

Equations (12) respect the formulation (1) with $\tilde{\boldsymbol{q}} = [\theta, \alpha]^{\mathsf{T}}$, $\boldsymbol{\delta} = [\delta_1, \delta_2, \delta_3]^{\mathsf{T}}$, $\boldsymbol{q}_c = [q_2, q_3, q_4]^{\mathsf{T}}$, and $\boldsymbol{q}_a = [q_1, q_5]^{\mathsf{T}}$, so the whole treatment depicted previously can be developed. It may

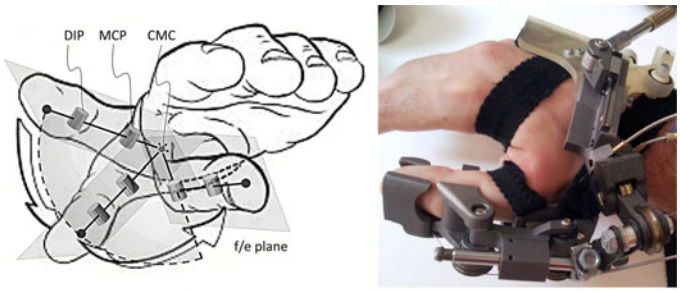


Fig. 6. HX thumb exoskeleton. (a) Thumb opposition as the revolution of its f/e plane around a frontal axis passing through the CMC joint; for complete opposition, the thumb also bends toward the palm, as in the figure, quitting the conic path. (b) Physical thumb exoskeleton.

be observed that, despite the additional DoFs $q_4$ and $q_5$, relation (11) remains valid, and that the $\alpha$ is fully driven only by the joint $q_4$: thus the torque $T_4$ will directly commute in the assistance torque to the a/a motion. In its current version, HX does not assist the MCP a/a angle, and all joints except $q_2$ and $q_3$ are passive.

### C. Thumb Kinematic Design

The thumb kinematic is different from the index finger one.

1) The thumb has a structure with three joints, still aligned on the f/e plane, but the root joint can execute 3-D motions.
2) The two f/e revolute joints are the MCP and DIP ones, while the first is the CMC [Carpo-Metacarpal, Fig. 6(a)] joint.
3) CMC joint allows for both f/e and a/a motions, and can compound them in the *opposition* movement. An interesting description of the CMC kinematics can be found in [36].

The thumb serial structure (CMC, MCP, and DIP f/e joints) lays on a plane rotating around an axis, which passes through the CMC center and is parallel to the middle finger metacarpus direction: when the thumb is extended, its tip can move along a conic path, the so-called thumb circumduction, Fig. 7(a). This thumb kinematic model—namely "surgeons' method" [39]—is simplified, the CMC mobility being more complex, but however describes efficiently the main functionality of the thumb, i.e., the *opposition* toward the long fingers.

The MCP and DIP f/e joints were addressed in a way similar to the index finger ones [19], [35], [36], through a $P\underline{RRR}$ kinematic architecture: design was based on the same assumptions, with the last $\underline{R}$ joint collocated with the DIP joint axis, and the $P\underline{RR}$ part realizing the self-alignment chain for the MCP, represented by the joints $J_{1,2,3}$ in Fig. 7(c).

The solution adopted in HX for the opposition employs the simplest among the remote center of motion systems (RCM [40]), the articulated parallelogram. The exoskeleton embeds three revolute joints in series, $J_{4,5,6}$ in Fig. 7(c), linked the CMC (the fourth one) through a frame worn on the thumb, Fig. 6(b). In order to work properly, the lengths $r$ and $l$ should be constant for each pair of the parallelogram linkages: in this

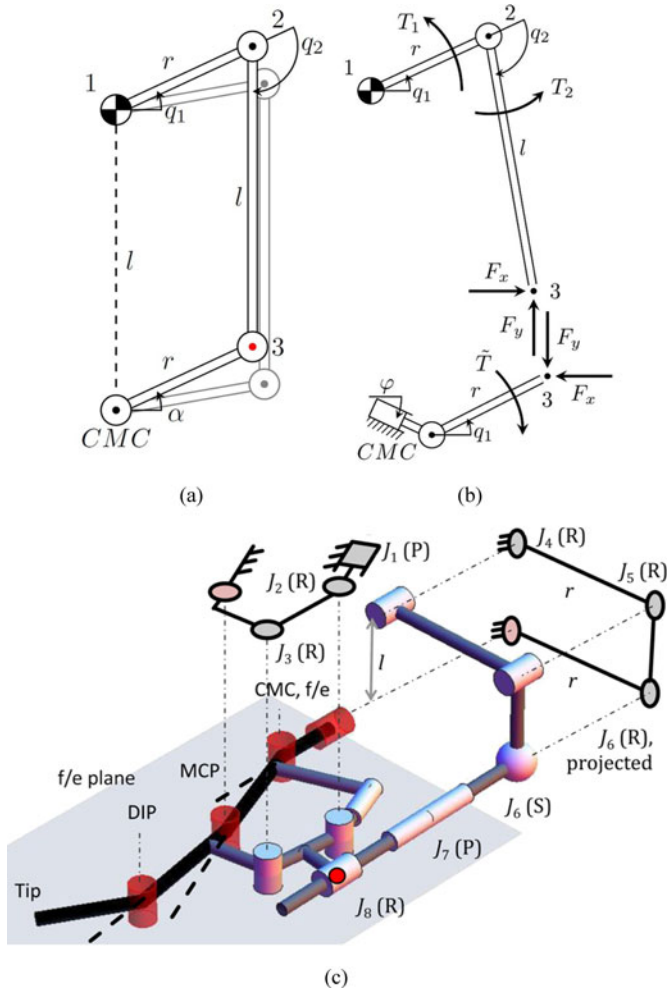


Fig. 7. HX thumb kinematic scheme. (a) Articulated parallelogram: joint 1 rotation is transmitted to the $CMC$ joint. (b) Free-body diagram for (a): if relation (13) holds, reaction along the slider supporting the CMC joint is zero. (c) Complete HX thumb kinematic scheme: the two projections (on the f/e plane, and normal to the opposition axis) show the equivalent joint disposition.

condition, the torque exerted at joint 1 is the same transferred to the CMC joint. Due to variations in user hand size and to the thumb f/e motion, a proper exoskeleton attachment point [see red dot in Fig. 7(a)] guaranteeing the parallelogram geometry is not available. Thus, the articulated parallelogram has been modified as in Fig. 7(c): the attachment point (red dot) lays on the f/e plane, lead by the $\overline{J_2J_3}$ member of the f/e chain, over a rotational joint $J_8$. The distance between this point and the parallelogram plane varies with flexion, so they are linked by an extensible member (prismatic joint $J_7$). The spherical joint $J_6$ matches the orientations of the $J_8$ axis with the parallelogram joints axis.

The articulated parallelogram is a particular case of the four-bar mechanism, so a proper actuation should obey to (8). In HX, a partial solution has been implemented, with the aim to avoid actuation of the third parallelogram joint $J_6$, realized through a passive ball–socket pair. It is still possible to deliver a torque $\tilde{T}$ onto the CMC, without generating on it a reaction force along a

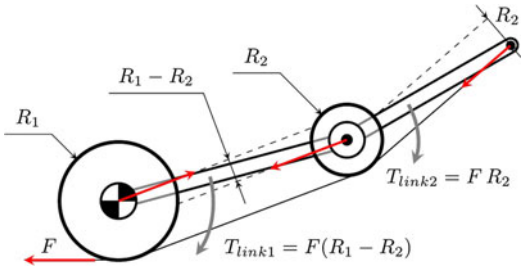


Fig. 8. Underactuated tendon-driven system: Differences in the the pulleys radii lead to torque splitting.

certain direction $\varphi$ [see Fig. 7(b)]

$$\begin{cases} T_1 = F_x(rs_1 + ls_{12}) - F_y(rc_1 + lc_{12}) \\ T_2 = F_x ls_{12} - F_y lc_{12} \end{cases}, \quad \begin{cases} \tilde{T} = F_x rs_1 - F_y rc_1 \\ 0 = F_x c_\varphi - F_y s_\varphi \end{cases}$$

$$\Downarrow \qquad\qquad \Downarrow$$

$$\begin{bmatrix} T_1 \\ T_2 \end{bmatrix} = \begin{bmatrix} rs_1 + ls_{12} & -rc_1 - lc_{12} \\ ls_{12} & -lc_{12} \end{bmatrix} \begin{bmatrix} F_x \\ F_y \end{bmatrix}, \quad \begin{bmatrix} F_x \\ F_y \end{bmatrix} = \frac{1}{rc_{1\varphi}} \begin{bmatrix} -s_\varphi & c_1 \\ -c_\varphi & s_1 \end{bmatrix} \begin{bmatrix} \tilde{T} \\ 0 \end{bmatrix}$$

$$\begin{bmatrix} T_1 \\ T_2 \end{bmatrix} = \frac{1}{rc_{1\varphi}} \begin{bmatrix} rc_{1\varphi} + lc_{12\varphi} & ls_2 \\ lc_{12\varphi} & ls_2 \end{bmatrix} \begin{bmatrix} \tilde{T} \\ 0 \end{bmatrix} \Rightarrow$$

$$\begin{cases} T_1 = \tilde{T}\left(1 + \dfrac{l\cos(q_1 + q_2 + \varphi)}{r\cos(q_1 + \varphi)}\right) \\ T_2 = \tilde{T}\dfrac{l\cos(q_1 + q_2 + \varphi)}{r\cos(q_1 + \varphi)}. \end{cases} \tag{13}$$

Equation (8) guaranteed the complete absence of reaction forces bearing the human joint, but required to address all the three exoskeleton revolute joints. Equation (13) shows that it is possible to nullify the $\varphi$ component of such reaction force, using two of the exoskeleton joints. However, $\varphi$ will depend upon the ratio $T_1/T_2$, and on $q_{1,2}$: further details are in Section III-A3. Moreover, by construction the scheme in Fig. 7(c) implies that also deviations of the CMC center along the opposition axis are absorbed by the self-aligning chain.

## III. Mechanics and Actuation

### A. Cable-Driven Underactuation

A widely adopted actuation strategy for robotic device is to remotely place the actuation system, and use flexible transmission means [21], [24], [29], [31], [36], [41], in order to decrease the inertia of the moving parts and to enhance the overall system portability and wearability. HX as well employs a cable-driven actuation system through flexible sheaths, namely *Bowden cables*. This choice comes from the fact that all HX active DoFs are of revolute kind: they can be driven by applying a tension force $F$ to a cable wrapped around a coaxial pulley of radius $R$, returning an applied torque $T = F\,R$. If the same cable travels through multiple pulleys, several joints can be driven, and by differentiation of pulley radii, it is possible to part the torque on each of the crossed joints: this is the *underactuation* strategy, which is the basic of both biological and robotic grasping [42], Fig. 8. Cables are hence referred also as *tendons*, and used in antagonist pairs with opposite wrapping direction in order to provide a bidirectional actuation.

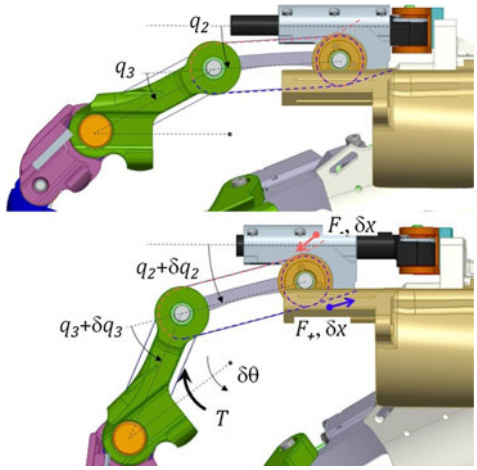


Fig. 9. Antagonistic cables actuating the MCP mechanism: the transmitted torque $T$ depends upon their differential tension $(F_+ - F_-)$ and the pulleys radius $R$. The first pulley (orange) is idle on its axis, while the second (green) is fixed on the phalanx link, thus cable position controls the global rotation $\theta$.

*1) MCP Flexion Transmission:* For both index and thumb the MCP f/e actuation is ruled by (11). The two joints $J_{2,3}$ of Fig. 5(a) are driven together by a single cable wrapped around two equal pulleys, with the Bowden sheaths capped in the rigid link between $J_1$ and $J_2$, Fig. 9: validity of this solution can be shown with a power balance argument [34]. From a static condition to another, a cables displacement $\delta x$ corresponds to joints variations $\delta q_2$, $\delta q_3$, and $\delta\theta = \delta q_2 + \delta q_3$. The cable path length is proportional to $q_2 + q_3$ via the radius $R$. Power conservation leads to

$$\begin{aligned} W_{\text{in}} &= (F_+ - F_-)\,\delta x = (F_+ - F_-)\,R(\delta q_2 + \delta q_3) = \\ &(F_+ - F_-)\,R\delta\theta = W_{out} = T\delta\theta \Rightarrow T = (F_+ - F_-)\,R; \\ W_{in} &= T\,(\delta q_2 + \delta q_3) = T_2\delta q_2 + T_3\delta q_3 \Rightarrow T_2 = T_3 = T \end{aligned} \tag{14}$$

where $T$ is the torque effectively transmitted to the MCP joint. The last line shows how this tendon system is equivalent to an actuation obeying (11).

*2) PIP-DIP Flexion Transmission:* The index PIP-DIP joints are underactuated by a single pair of tendons. Driving them till the PIP joint by a pair of Bowden hoses would result in the flexible sheaths moving around the exoskeleton when the MCP joint rotates. In HX, instead, all the Bowden hoses are terminated at the same level, with the tendons for the MCP on the internal side and the ones for the P-DIP on the external side Fig. 5(c). In order to not affect the MCP actuation, the pulleys of the P-DIP on the $J_{2,3}$ axes are equal (see Fig. 10(b), $R_0^{FGR}$ and $R_1^{FGR}$). This architecture greatly minimizes the sheath encumbrance and bending, and balances the two sides of the exoskeleton. For the thumb DIP joint, the same tendons used for the MCP are employed, so the DIP pulley is smaller than the two other ones (see Fig. 10(b), $R_0^{THB}$ and $R_1^{THB}$).

*3) Opposition Transmission:* This is ruled by (13), which can lead to a variety of solutions. With a tendon-driven underactuated system, the ratio between $T_1$ and $T_2$ can be chosen through the pulleys radii, obtaining various $\varphi$: examples are

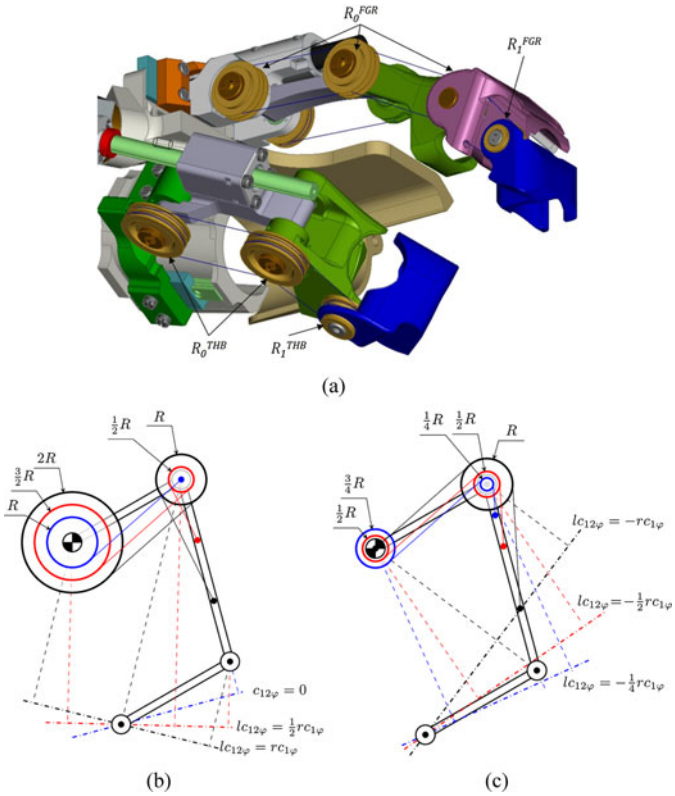


Fig. 10. Underactuated tendon-driven architectures. (a) The cable of the index P-DIP joints crosses the pulleys, but only conveys torque to the middle (violet) and distal (blue) phalanges; the cable of the thumb drives both MCP and DIP joints. (b-c) Underactuated architectures for the CMC parallelogram, depicted with different colors: in all of them, the torque $\tilde{T} = T_1 - T_2$ delivered to the CMC is equal to the tendon force multiplied by $R$. (b) Positive ratio: as $\varphi$ (dashdotted line) tilts, both the radii increase, with their difference constantly equal to $R$. (c) Negative ratio: as $\varphi$ tilts, the radii vary with their sum constantly equal to $R$.

reported in Fig. 10(b), (c), with positive and negative torque ratios. It is worth noting that a *negative* ratio [cable wrapping direction is inverted, Fig. 10(c)] permits to convey the same torque to the CMC with smaller pulleys. HX adopts the solution with inverted wrapping and equal pulleys (see Fig. 10(c), red), in order to minimize the encumbrance. However, the dashdotted lines in Fig. 10(b), (c) will move as the mechanism moves, obeying their labeling equations: if it is requested to achieve a constant direction with no reaction force, the ratio $T_1/T_2$ should vary with joints $q_{1,2}$, thus the pulleys should be shaped in a proper cam profile.

### B. Actuation System

The HX remote actuation unit (see Fig. 11) is a series of four identical actuation lines, one for each global DoF (index MCP and P-DIP, and thumb MCP-DIP, and opposition). On each actuation line a dc-motor (Faulhaber 1331T006SR, 3.11 W, 6 V with incremental encoder IE2-400, 14:1 planetary gearhead) transmits its shaft rotation to two leadscrews with opposite threads, through a spur gear stage. The nuts of the leadscrews then move in opposite direction, and this antagonistic linear motion is converted by means of cables in a capstan rotation. The tendons

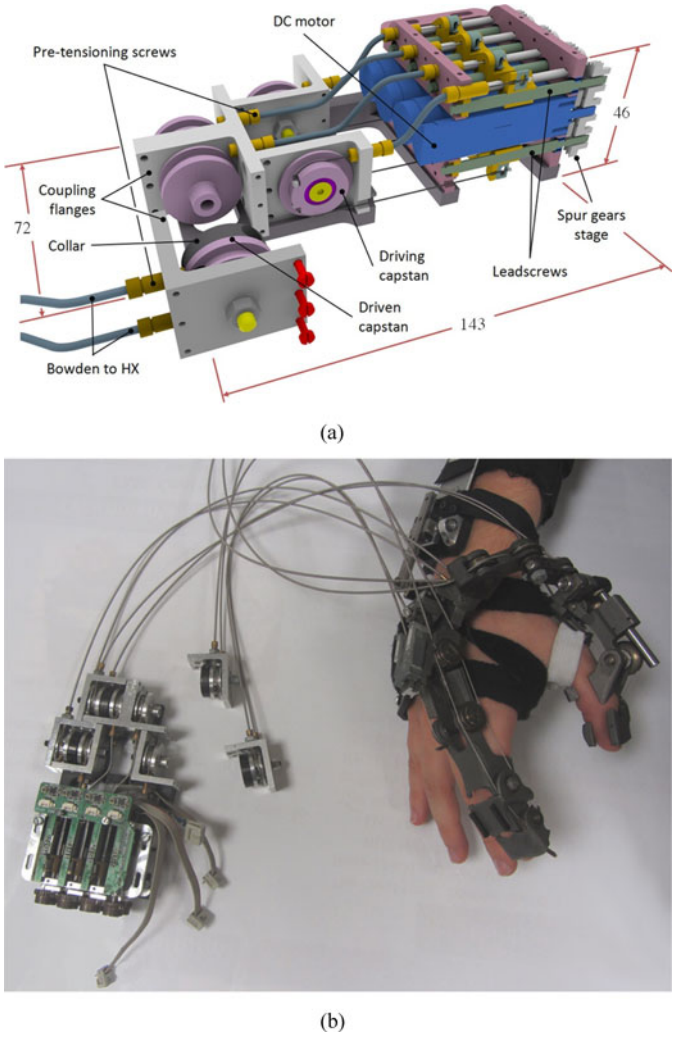


Fig. 11. Remote actuation unit and removable capstan system, [34]. (a) CAD with encumbrances and cross-section view of a single actuation line. (b) Real actuator (left), detachable pulleys (center) and tethered worn HX (right).

transmitting the motion to HX are capped in a similar capstan, Fig. 11(a). The driving capstan, attached to the motor tendons, and the driven capstan, attached to the HX tendons, are designed in order to be mated together: once their flange are aligned, a hollow collar can be tighten to lock together the two rotating elements. This pluggable coupling system is a fast and reliable solution augmenting the HX usability: not only it simplifies and speed-up the don/doff phases, but also gives the possibility to use HX without actuation system, thus only as a measuring/assessing device, or to mate it with other actuators. At the extremities of each sheaths, screws are provided in order to regulate the tendons pretension.

### C. Controller

The control system of the HX has a hierarchical architecture divided in two layers, both running on a commercial system (sbRIO-9632, National Instruments, TX, USA), endowed with a real-time 400-MHz processor and a field-programmable gate array (FPGA) processor. The high-level controller runs on the

real-time processor at 100 Hz and coordinates all the active DoFs: it converts the desired hand task into motor position reference. The low-level controller consists of a four independent position loops running at 100 Hz and four commercial servo controllers (EPOS2 24/2, Maxon Motors, CH) running a velocity control loop at 1 kHz. The two layers are interfaced together by means of a CAN bus. For each control loop, error between reference and measured motor positions is converted into a desired motor velocity and sent through CAN bus to the servo controllers.

## IV. Assessment of Self-Alignment

An assessment of the self-aligning performances of MCP mechanism on the index module has been executed through a motion tracking system. The protocol required HX to execute straight-index f/e tasks, while worn by a passive user. Hand of the subjects and HX joints positions were tracked by means of infrared reflective marker identification through an acquisition system (460 Motion Capture Datastation, VICON, CO, USA) equipped with six high-speed cameras (TM-6710CL, Pulnix, CA, USA) working at a frequency of 120 Hz.

### A. Experimental Protocol

Four healthy subjects (age 25–28) volunteered to participate this study after they signed an informed consent. Each subject worn the HX hand dorsal module, tightly fit to the subject hand. During the acquisition, the kinematic reference was given by three markers fixed on the dorsal module (bigger markers in Fig. 12(a), (b)), and never removed throughout the whole protocol. The protocol was divided in two sessions: in the first the subject autonomously executed f/e tasks with the straight index finger. Trajectories of the four markers attached to the finger [one for each joint plus one for the fingertip, Fig. 12(a)] were used to extract the associated angles. At the end of the session such markers, except for the fingertip one, were removed (see Fig. 12(b): reference markers did not change, and one additional marker was attached to the a/a slider) and the HX finger module was worn, with its own markers (five in total) aligned along the medial plane and in given position over the structure [see Fig. 12(c)]. In the second session, HX executed f/e tasks while its joints trajectories were acquired, while the subject was asked to be passively driven by the device without opposing the motion. There were a total of 10 markers in this session: an example of trajectories reconstructed from raw data is shown in Fig. 12(d).

### B. Data Analysis

It was difficult to acquire both the HX and the hand kinematic at the same time, since there was not enough room for positioning additional markers and allowing them to be always visible to at least three over six cameras. In order to evaluate the kinematic discrepancy, data from the two sessions were crossed in the following manner. The first session was used to reconstruct the natural MCP center positions $MCP_h$ as function of the MCP angle $\theta$, thus identifying the functions $\delta_i(\theta)$, $i = \{1, 2, 3\}$. The second session was used to reconstruct the set

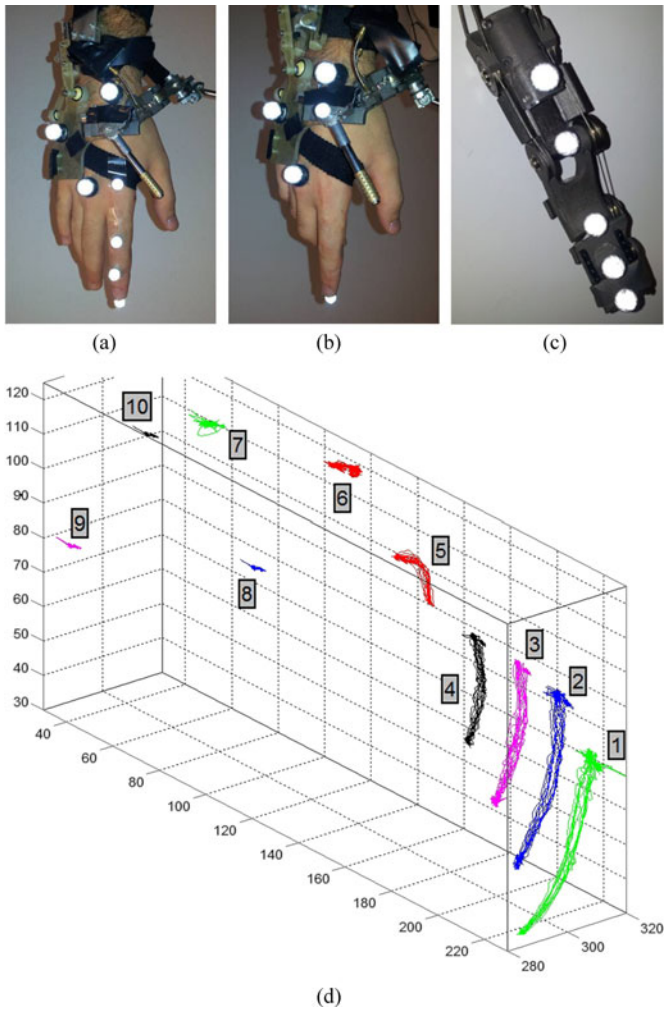


Fig. 12. Visual acquisition markers, for bare-hand session (a) and for HX session, disposed on the hand (b, markers 1 and 7 to 10) and on HX (c, markers 2 to 6). (d) 3-D reconstruction of a HX sessions with multiple f/e trials from raw data, with labeled trajectories.

of HX DoFs $q_i$, from which it was possible to extrapolate MCP position $MCP_{HX}$ and angle $\theta_{HX}$, as seen from HX: following (12) the angle $\theta_{HX}$ was assumed as $q_{23} + \pi/2$. The *expected* position of the natural MCP axis was calculated using the $\delta_i$, $i = \{1, 2, 3\}$ functions, evaluated on the $\theta_{HX}$ angle. Difference between the two MCP joint positions for a given subject are reported in Fig. 13(a). Knowing the fingertip position thanks to the related marker (the same in both sessions) it was possible to extrapolate the MCP flexion angle associated with the hand $\theta_h$ as the tilt of the vector joining $MCP_h$ with the fingertip. In Fig. 13(b), (c) the discrepancy between $\theta_{HX}$ and $\theta_h$ is reported.

### C. Results

Each session comprised multiple repetitions of f/e tasks, separated by fully extended and fully flexed phases. The starting position for the VICON static setting corresponded to the extended condition: due to this, the calculated error is almost zero for $\theta = 0$. The discrepancy between $MCP_{HX}$ and $MCP_h$ shown in Fig. 13(a) is quite small (a few decimals of millimeter)

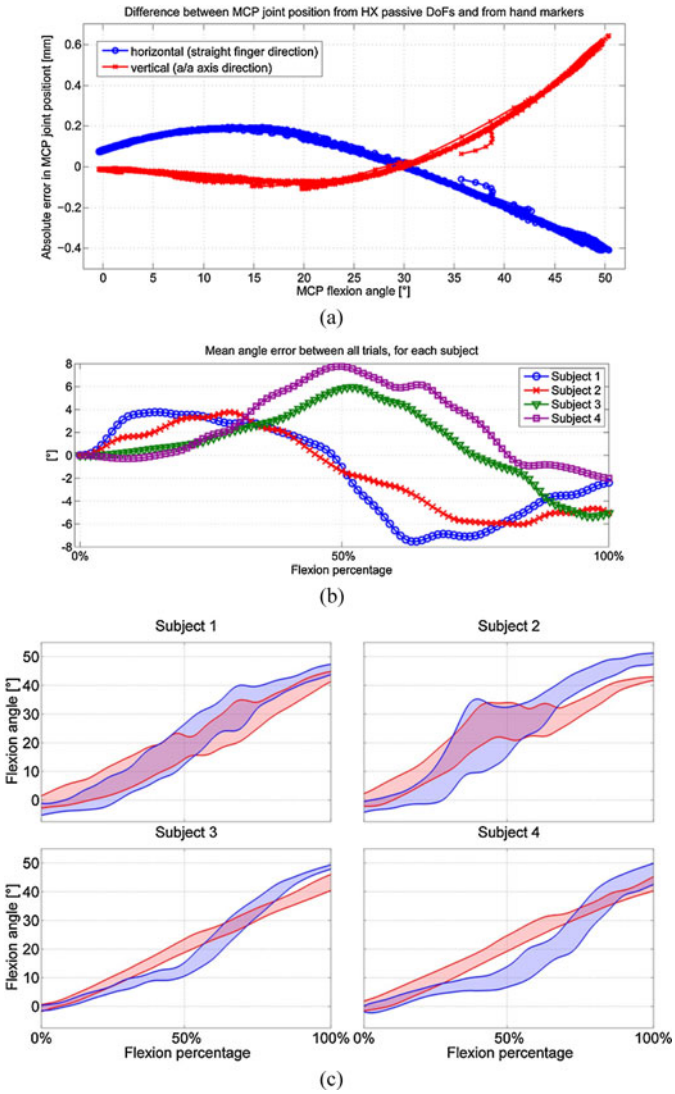


Fig. 13. Results. (a) Difference between the MCP position as calculated from HX DoFs through (12) and the naked hand tracing: the deviation along the direction normal to the f/e plane was negligible, and is not reported. (b) MCP flexion angle mean error between HX and the hand for each subject. (c) Envelope of motion profiles for each subject (12 trials for each subject), of both HX (red) and hand (blue) MCP flexion angle.

and repetitive along all trials, meaning that the formulation (12) used for the calculation of the two MCP positions is consistent with the device. Other subjects showed similar results.

Fig. 13(b) shows, for each subject, the difference between $\theta_{HX}$ and $\theta_h$, considered only in the moving phases (extension and flexion, without considering the static phases at fully extended or fully flexed), and mediated among all trials. The plot shows bigger errors in the central phase, with peaks of $8^\circ$, while a static error at flexed position of $5^\circ$: in general, the error is quite well contained. Additional errors may be caused by the data analysis, mainly in the assumed fact that the $\delta_i$, $i = \{1, 2, 3\}$ functions are the *same* with and without HX: it may be expected that fitting the regulations and the straps of HX on the hand slightly modifies the hand attitude itself.

Fig. 13(c) reports one graph for each subject, plotting the envelope of $\theta_{HX}$ (red) and $\theta_h$ (blue) among *all* the moving trials: the colored stripes are centered on the mean value of the angle, with the width three times the standard deviation. The error between the exoskeleton and the hand that can be deduced from these graphs is more depreciative than the one in Fig. 13(b), since each trial is mixed with all the others, but they give a global feedback over the HX reliability. In fact, the red envelope should be as close as possible to a straight line, in accordance with the commanded flexion percentage: subject 2 showed the worst performance, but in general the behavior is acceptable, and fluctuations may be due to errors in VICON acquisition and the reconstruction noise, or to nonlinearities in the flexible sheath transmission. The difference between the blue and red envelope gives information about the exoskeleton stability: for all subjects at the beginning and at the end of the trials, the hand angle is flatter than the robotic one. The main explanation of this fact is that the compliance of the finger tissue inside the exoskeleton phalangeal shells "slows down" the interaction whenever HX begins to move from a static condition.

## V. Discussion and Conclusion

In this paper, a novel wearable robotic exoskeleton for the hand has been presented: HX is a modular platform, divided in the index finger, thumb finger, and hand dorsal modules. It has a total of DoFs, seven for the index (three passive, four active) and nine for the thumb motions (six passive, three active). Active joints are underactuated by means of tendon-sheaths driving systems, resulting in four global independent motions: the index MCP and D-PIP f/e, and the thumb MCP-DIP f/e and opposition. An external self-standing module hosts the actuation, with four identical motors. Weights of the various modules are index 118 g, thumb 151 g, hand dorsal module (including opposition chain) 169 g, for a total of 438 g laying on the hand; wrist cuff 135 g, Bowden sheaths with detachable pulleys 205 g, for a total of 340 g laying on the forearm; actuator 494 g.

The theoretical framework of self-alignment [13] underlying the HX design has been briefly recapped: its application to devices from the state of the art shown in Section II-A sustains the advantages of such methodology in analyzing wearable robot architectures. This methodology resembles the hybridization design [6], as it treats as a whole the *kinematic* of an exoskeleton structure, for the human compatibility, and the *actuation*, for the robot effectiveness, while usually these two aspects are faced separately. The methodology can be collected within the resilient system concept [32], as a particular case in which the balanced state, corresponding to alignment between robotic and human joints, is achieved autonomously thanks to the arrangement of the passive DoFs and to the actuation of the active ones—respectively, (1) and (2).

The passive DoFs for index MCP joint self-alignment can absorb any misplacement of its center, thus a calibration phase is not required in the orthosis fitting. Moreover, the a/a motion is permitted, achieving a full mobility of the index (see Section II-B). The thumb MCP joint is treated alike, with a kinematic chain conceptually identical to the index one. Section IV presented an assessment of the MCP f/e motion assistance, based on experiments carried on with healthy subjects, where free-hand

TABLE I
COMPARISON WITH OTHER HAND EXOSKELETONS: HX CONJUGATES INDEX A/A, THUMB OPPOSITION, SELF-ALIGNMENT AND PORTABILITY

| | **HEXORR [17]** | **HIFE [18]** | **[37]** | **HandSOME [19]** | **CAFE [20], [21]** | **HANDEXOS [31]** | **[24]** | **[26]** | **iHandRehab [36]** | **[27]** | **HX** |
|---|---|---|---|---|---|---|---|---|---|---|---|
| **Index**[a] | f/e(1) | f/e(2) | f/e | Straight fingers grasp (1) | f/e | f/e | f/e | f/e | f/e, a/a | f/e(2), a/a | f/e(2), pas. a/a |
| **Thumb**[a] | f/e(1) adjust. a/a | — | f/e(1) oppos. | | — | — | — | f/e(1), a/a | f/e, a/a | f/e(2), a/a | f/e(1), oppos. |
| **Weight**[b] | — | — | — | 130 g | 140 g | 110 g | — | — | 250 g | 1 kg | 270 g |
| **Max size**[c] | — | — | — | — | 4 cm | 2 cm | 4 cm | 3 cm | 4 cm | 5 cm | 3 cm |
| **Features** | Direct match | End-point | 4-bar | RCM | Direct match | Multi-DoF | 4-bar | Direct match | 4-bar | RCM | Self-alignment |
| | Fixed frame, no reach-to-grasp | | | | Single finger exoskeletons | | | Full hand | Index and thumb exoskeletons | | |

[a](#) = no. of independent DoFs, if underactuated. [b]Weights refer to moving parts only. [c]Max size refers to the biggest dorsal encumbrance.

movements were compared with HX driven ones. Data show a limited error of the MCP joint angle, maximized in accelerating and decelerating phases of the exoskeleton: this error is due to the compliance of the finger tissue inside the exoskeleton shells, which damps the interaction whenever HX starts or stops its motion, and can be restrained with a better adaptation to the finger transverse dimensions (e.g., personalized internal layers).

A solution for the thumb opposition has been presented in Section II-C. The solution exploits a RCM with an articulated parallelogram extended for the 3-D motion of the thumb. We demonstrated how it can absorb misalignment of the CMC center along the $\varphi$ direction (Section III-A3 showed how the parallelogram design can be "tuned" to adjust such direction) and along the opposition axis. Despite not being a complete solution, as the one for the MCP, the proposed mechanism is a novel self-aligning thumb exoskeleton, including the validated MCP f/e self-alignment mechanism with the opposition articulated parallelogram. With reference to Table I, thumb *opposition* and *a/a* are different motions: the thumb a/a is a rotation around an axis through the CMC center, almost parallel to the lateral–medial direction [39], and so does not "oppose" the thumb toward the palm.

The actuator presented in Section III has a compact and portable design: its main drawbacks are the nonbackdrivability, the limited stroke, and the low power. However, for the aim of this paper, this actuator has been successfully used in the validation trials. An important novelty in the HX transmission design is the presence of a detachable stage, realized by pairs of mating capstans. This stage allows HX to be easily disconnected from its mechanical power source, and to be used with different actuators, drastically increasing the device flexibility.

Future works will concern the development of a new actuator with higher performances, a review of the wearable modules with sensors integration, and a dedicated validation for the thumb opposition system, while results in this paper suggest that the current index architecture can be successfully replicated. Complexity and size of HX are still limiting for a real use, but are not bigger than those of analogous exoskeletons: in particular, dorsal encumbrance is really limited. A major difference is that the passive DoFs of HX are used not only as joint misalignment countermeasure, but also allows easily to detach and assemble the various modules, easing the donning and doffing procedure and augmenting the flexibility. Regarding the weight, it is hard to find comparison in the state of the art, some numbers are given in Table I. As general indication, Aubin *et al.* determined that a device deployed on the hand should not exceed 0.5 kg [43], which is compatible with the weight of the wearable modules of HX. Next development of the design will also consider optimization of structural material distribution. Next development of the design will also consider optimization of structural material distribution: the exoskeleton links have been produced via selective laser melting (SLM) of Titanium alloy powder (Ti6Al4V), allowing freedom in their 3D shapes, at no additional cost. It is worth to note that in this kind of addictive manufacturing process the working area is fixed, and thus costs can be dramatically cut by printing several samples of the device into the same tray.

## REFERENCES


[1] H. Kazerooni, "Exoskeletons for human power augmentation," in *Proc. IEEE/RSJ Int. Conf. Intell. Robots Syst.*, 2005, pp. 3120–3125.

[2] R. Bogue, "Exoskeletons and robotic prosthetics: A review of recent developments," *Ind. Robot, Int. J.*, vol. 36, no. 5, pp. 421–427, Aug. 2009.

[3] G. Kwakkel, B. J. Kollen, and H. I. Krebs, "Effects of robot-assisted therapy on upper limb recovery after stroke: A systematic review," *Neurorehabil. Neural Repair*, vol. 22, no. 2, pp. 111–121, Jan. 2008.

[4] M. Canela, A. J. del Ama, and J. L. Pons, "Design of a pediatric exoskeleton for the rehabilitation of the physical disabilities caused by cerebral palsy," *Biosyst. Biorobot.*, vol. 1, pp. 255–258, 2013.

[5] J. L. Pons, "Rehabilitation exoskeletal robotics. The promise of an emerging field," *IEEE Eng. Med. Biol. Mag.*, vol. 29, no. 3, pp. 57–63, May/Jun. 2010.

[6] W. Zhang, P. Ouyang, and Z. Sun, "A novel hybridization design principle for intelligent mechatronics systems," in *Proc. Int. Conf. Adv. Mechatronics*, 2010, pp. 4–6.

[7] N. Hogan, H. Krebs, J. Charnnarong *et al.*, "MIT-MANUS: A workstation for manual therapy and training," in *Proc. IEEE Int. Workshop Robot Human Commun.*, 1992, pp. 161–165.

[8] M. Cirstea and M. F. Levin, "Compensatory strategies for reaching in stroke," *Brain*, vol. 123, no. 5, pp. 940–953, 2000.

[9] N. Karnati, B. Kent, and E. Engeberg, "Bioinspired sinusoidal finger joint synergies for a dexterous robotic hand to screw and unscrew objects with different diameters," *IEEE/ASME Trans. Mechatronics*, vol. 18, no. 2, pp. 612–623, Apr. 2013.

[10] A. Stienen, E. Hekman, F. Van Der Helm *et al.*, "Self-aligning exoskeleton axes through decoupling of joint rotations and translations," *IEEE Trans. Robot.*, vol. 25, no. 3, pp. 628–633, Jun. 2009.

[11] N. Vitiello, T. Lenzi, S. Roccella *et al.*, "NEUROExos: A powered elbow exoskeleton for physical rehabilitation," *IEEE Trans. Robot.*, vol. 29, no. 1, pp. 220–235, Feb. 2013.

[12] Z. Ju and H. Liu, "Human hand motion analysis with multisensory information," *IEEE/ASME Trans. Mechatronics*, vol. 19, no. 2, pp. 456–466, Apr. 2014.

[13] M. Cempini, S. M. M. De Rossi, T. Lenzi *et al.*, "Self-alignment mechanisms for assistive wearable robots: A kinetostatic compatibility method," *IEEE Trans. Robot.*, vol. 29, no. 1, pp. 236–250, Feb. 2013.
[14] A. De Santis, B. Siciliano, A. De Luca *et al.*, "An atlas of physical human robot interaction," *Mechanism Mach. Theory*, vol. 43, no. 3, pp. 253–270, Mar. 2008.
[15] P. Heo, G. M. Gu, S.-J. Lee *et al.*, "Current hand exoskeleton technologies for rehabilitation and assistive engineering," *Int. J. Precis. Eng. Manuf.*, vol. 13, no. 5, pp. 807–824, May 2012.
[16] E. R. Kandel, J. H. Schwartz, T. M. Jessel *et al.*, *Principles of Neural Science*. vol. 4, New York, NY, USA: McGraw-Hill, 2000.
[17] C. N. Schabowsky, S. B. Godfrey, R. J. Holley *et al.*, "Development and pilot testing of HEXORR: Hand exoskeleton rehabilitation robot.," *J. Neuroeng. Rehabil.*, vol. 7, pp. 36–51, Jan. 2010.
[18] U. Mali and M. Munih, "HIFE-haptic interface for finger exercise," *IEEE/ASME Trans. Mechatronics*, vol. 11, no. 1, pp. 93–102, Feb. 2006.
[19] E. B. Brokaw, I. Black, R. J. Holley *et al.*, "Hand Spring Operated Movement Enhancer (HandSOME): A portable, passive hand exoskeleton for stroke rehabilitation.," *IEEE Trans. Neural Syst. Rehabil. Eng.*, vol. 19, no. 4, pp. 391–399, Aug. 2011.
[20] T. Worsnopp, M. Peshkin, J. Colgate *et al.*, "An actuated finger exoskeleton for hand rehabilitation following stroke," in *Proc. IEEE 10th Int. Conf. Rehabil. Robot.*, Jun. 2007, pp. 896–901.
[21] C. Jones, F. Wang, R. Morrison *et al.*, "Design and development of the cable actuated finger exoskeleton for hand rehabilitation following stroke," *IEEE/ASME Trans. Mechatronics*, vol. 19, no. 1, pp. 131–140, Feb. 2014.
[22] A. Schiele and F. C. T. van der Helm, "Kinematic design to improve ergonomics in human machine interaction," *IEEE Trans. Neural Syst. Rehabil. Eng.*, vol. 14, no. 4, pp. 456–69, Dec. 2006.
[23] J. Iqbal, N. G. Tsagarakis, and D. G. Caldwell, "A human hand compatible optimized exoskeleton system," in *Proc. IEEE Int. Conf. Robot. Biomimetics*, 2010, pp. 685–690.
[24] A. Wege, K. Kondak, and G. Hommel, "Force control strategy for a hand exoskeleton based on sliding mode position control," in *Proc. IEEE/RSJ Int. Conf. Intell. Robots Syst.*, Oct. 2006, pp. 4615–4620.
[25] L. Lucas, M. Dicicco, and Y. Matsuoka, "An EMG-controlled hand exoskeleton for natural pinching," *J. Robot. Mechatron.*, vol. 16, pp. 482–488, 2004.
[26] Y. Hasegawa, Y. Mikami, K. Watanabe *et al.*, "Five-fingered assistive hand with mechanical compliance of human finger," in *Proc. IEEE Int. Conf. Robot. Autom.*, May 2008, pp. 718–724.
[27] M. Fontana, A. Dettori, F. Salsedo *et al.*, "Mechanical design of a novel hand exoskeleton for accurate force displaying," in *Proc. IEEE Int. Conf. Robot. Autom.*, May 2009, pp. 1704–1709.
[28] H. In, K.-J. Cho, K. Kim *et al.*, "Jointless structure and under-actuation mechanism for compact hand exoskeleton," in *Proc. IEEE 12th Int. Conf. Rehabil. Robot.*, 2011, pp. 1–6.
[29] Y. Kadowaki, T. Noritsugu, M. Takaiwa *et al.*, "Development of soft power-assist glove and control based on human intent," *J. Robot. Mechatron.*, vol. 23, no. 2, pp. 281–291, 2011.
[30] N. Jarrasse and G. Morel, "Connecting a Human Limb to an Exoskeleton," *IEEE Trans. Robot.*, vol. 28, no. 3, pp. 697–709, Jun. 2012.
[31] A. Chiri, N. Vitiello, F. Giovacchini *et al.*, "Mechatronic design and characterization of the index finger module of a hand exoskeleton for post-stroke rehabilitation," *IEEE/ASME Trans. Mechatronics*, vol. 17, no. 5, pp. 884–894, Oct. 2012.
[32] Z.-H. Sun, G. Yang, B. Zhang *et al.*, "On the concept of the resilient machine," in *Proc. 6th IEEE Conf. Ind. Electron. Appl.*, 2011, pp. 357–360.
[33] M. Cempini, N. Vitiello, and F. Giovacchini *et al.*, "Wearable Exoskeleton device for hand rehabilitation," PCT Patent PCT/IB2013/056894, Mar. 6, 2014.
[34] M. Cempini, S. M. M. De Rossi, T. Lenzi *et al.*, "Kinematic and design of a portable and wearable exoskeleton for hand rehabilitation," in *Proc. IEEE 13th Int. Conf. Rehabil. Robot.*, 2013, pp. 1–6.
[35] J. Li, R. Zheng, Y. Zhang *et al.*, "iHandRehab: An interactive hand exoskeleton for active and passive rehabilitation," in *Proc. IEEE 12th Int. Conf. Rehabil. Robot.*, 2011, pp. 1–6.
[36] S. Ueki, H. Kawasaki, S. Ito *et al.*, "Development of a hand-assist robot with multi-degrees-of-freedom for rehabilitation therapy," *IEEE/ASME Trans. Mechatronics*, vol. 17, no. 1, pp. 136–146, Feb. 2012.
[37] E. Chao, K.-N. An, W. Coone *et al.*, *Biomechanics of the Hand: A Basic Research Study*. Singapore: World Scientific, 1989.
[38] P. Gad, "The anatomy of the volar part of the capsules of the finger joints," *J. Bone Joint Surg. B*, vol. 49, pp. 362–367, 1967.
[39] A. I. Kapandji, "Clinical evaluation of the thumb's opposition," *J. Hand Ther.*, vol. 5, no. 2, pp. 102–106, 1992.
[40] G. Zong, X. Pei, J. Yu *et al.*, "Classification and type synthesis of 1-DOF remote center of motion mechanisms," *Mech. Mach. Theory*, vol. 43, no. 12, pp. 1585–1595, Dec. 2008.
[41] N. Vitiello, T. Lenzi, S. M. M. De Rossi *et al.*, "A sensorless torque control for antagonistic driven compliant joints," *Mechatronics*, vol. 20, no. 3, pp. 355–367, 2010.
[42] V. Lippiello, F. Ruggiero, B. Siciliano *et al.*, "Visual grasp planning for unknown objects using a multifingered robotic hand," *IEEE/ASME Trans. Mechatronics*, vol. 18, no. 3, pp. 1050–1059, Jun. 2013.
[43] P. Aubin, H. Sallum, C. Walsh *et al.*, "A pediatric robotic thumb exoskeleton for at-home rehabilitation: The isolated orthosis for thumb actuation (IOTA)," in *Proc. IEEE Int. Conf. Rehabil. Robot.*, Jun. 2013, pp. 1–6.

**Marco Cempini** (S'11) received the M.Sc. degree (*cum laude*) in aeronautical engineering jointly from the University of Pisa, Pisa, Italy, and from Scuola Superiore Sant'Anna, Pisa, Italy, in 2010. He is currently working toward the Ph.D. degree in biorobotics at the BioRobotics Institute, Scuola Superiore Sant'Anna.

He has been a Visiting Student at the Robotics and Mechatronics Laboratory of the University of Twente, Enschede, The Netherlands. His current research interests include mechanical design, modeling, and development for wearable robotics, oriented towards upper and lower limb assistance.

Mr. Cempini participated in the first ESA Lunar Robotics Challenge in 2008.

**Mario Cortese** received the M.Sc. degree (*cum laude*) in electronic engineering from the University of Pisa, Pisa, Italy, in 2011. He is currently working toward the Ph.D. degree in biorobotics at the BioRobotics Institute, Scuola Superiore SantAnna, Pisa, Italy.

His current research interests include electronic design for wearable robotics, development of human–robot interfaces, and control strategies for upper and lower limb rehabilitation robots.

**Nicola Vitiello** (M'12) received the M.Sc. degree (*cum laude*) in biomedical engineering from the University of Pisa, Pisa, Italy, in 2006, and from the Scuola Superiore SantAnna, Pisa, Italy, in 2007, from where he also received the Ph.D. degree in biorobotics in 2010.

He is currently an Assistant Professor with the BioRobotics Institute, Scuola Superiore SantAnna, where he leads the Wearable Robotics Laboratory. He is the author or coauthor of 22 ISI/Scopus papers and 30 peer-reviewed conference proceedings papers. He has served as the Scientific Secretary of the EU FP7 CA-RoboCom project, and he is currently the Project Coordinator of the EU FP7 CYBERLEGs Project, the IUVO Project funded by Fondazione Pisa, and the EARLYREHAB Project funded by the Regione Toscana. His main research interests include the development of wearable robotic devices for human motion assistance and rehabilitation and of robotic platforms for neuroscientific investigations. In 2006, he participated in the ninth ESA Student Parabolic Flight Campaign. In 2008, he participated in the 1st ESA Lunar Robotics Challenge as a Ph.D. Student.